Numerical Simulation Of Impact Tests On Gfrp Composite Laminates

Costantino Menna, Domenico Asprone, Giancarlo Caprino, Valentina Lopresto, Andrea Prota

Accepted Manuscript

Title: Numerical Simulation Of Impact Tests On Gfrp Composite Laminates

Authors: Costantino menna, Domenico asprone, Giancarlo caprino, Valentina lopresto, Andrea prota

PII: S0734-743X(11)00056-X

DOI: 10.1016/j.ijimpeng.2011.03.003

Reference: IE 1985

To appear in: *International Journal of Impact Engineering*

Received Date: 8 January 2011

Revised Date: 4 March 2011

Accepted Date: 19 March 2011

Please cite this article as: menna C, asprone D, caprino G, lopresto V, prota A. Numerical Simulation Of Impact Tests On Gfrp Composite Laminates, International Journal of Impact Engineering (2011), doi: 10.1016/j.ijimpeng.2011.03.003

NUMERICAL SIMULATION OF IMPACT TESTS ON GFRP COMPOSITE LAMINATES

Costantino MENNA[1°], Domenico ASPRONE[1], Giancarlo CAPRINO[2], Valentina LOPRESTO[2], Andrea PROTA[1]

[1]Department of Structural Engineering - University of Naples "Federico II", Naples, Italy
[2]Department of Materials and Production Engineering - University of Naples "Federico II", Naples, Italy

ABSTRACT

The design of advanced composite structures or components subjected to dynamic loadings requires a deep understanding of the damage and degradation mechanisms occurring within the composite material. The present paper deals with the numerical simulation of low-velocity impact tests on glass fabric/epoxy laminates through the LS-DYNA Finite Element (FE) code. Two laminates of different thickness were subjected to transverse impact at different energy levels and modelled by FE. Solid finite elements combined with orthotropic failure criteria were used to model the composite failure and stress based contact failure between plies were adopted to model the delamination mechanism. The final simulation results showed a good correlation with experimental data in terms of both force-displacement curves and material damage.

Keywords: Low velocity impact, GFRP, LS-DYNA, composite failure, delamination

INTRODUCTION

°Corresponding author: via Claudio, 21 80125 – Naples, Italy
email: costantino.menna@unina.it - tel: +39 081 7683672 - fax: +39 081 7683491

The use of fibre-reinforced composite materials has increased over the last decades, due to their advantageous specific mechanical properties and corrosion resistance. Advanced composites have been used in many different engineering applications encompassing military, automotive and naval industry, and especially in aerospace, where weight reduction is one of the most important design parameters. Although these materials offer very attractive properties, their application is often restricted by their vulnerability to transverse impact [1], forcing the adoption of large safety factors and resulting in significantly over-designed structures.

Aeronautical components are prone during service to foreign object impact events [1] varying in the range of low to high velocities and impacting masses, consisting of dropping tools during production, repair or maintenance operations, ice particles or runway debris, bird strikes. At high velocity, the structural response is dominated by the stress wave propagation through the thickness of the laminate, and the resultant damage is quite localized. On the contrary, in a low-velocity impact the contact duration is long enough to excite the global structural response, leading to a more diffuse damage [2,3].

The damage suffered by a composite laminate subjected to impact loading can be divided into four distinct categories: matrix cracking, delamination between adjacent plies, fibre breakage, and perforation. Such order corresponds to the damage sequence occurring for increasing impact energies. In particular, delamination, occurring at moderately low energy levels, deserves serious considerations, being able to cause a significant decrease in the static material compression strength, or growing under cyclic loads leading to a gradual loss in strength and stiffness [4].

The impact response of composite laminates has been widely treated in the literature by experimental research works, analytical formulations and numerical implementations, with the objectives of understanding the tup-material interaction [5,6], predicting the extent of induced damage [7,8], and estimating the residual properties of the structure [4,9,10]. In particular, many research efforts have been spent to model impact history. To this aim, quite simple closed-form solutions [11], easy to use and effective, but restricted to simple impact cases due to the underlying simplifying assumptions [7,11,12], have been often employed.

In the last decades, an alternative to the analytical formulations has been offered by the numerical methodologies based on Finite Element (FE) approach. Since the onset of damage in a composite does not usually lead to ultimate failure, the ability of FE in simulating an impact event is critically dependent on its capacity to represent the sequence of damage modes, the conditions for delamination propagation, as well asthe stiffness and strength degradation associated with the various damage states.

FE simulation works available in the literature are based on different theoretical formulations including failure criteria, plasticity theory, fracture mechanics, and damage mechanics. The main drawback of the failure criteria approach [13], initially adopted for unidirectional composites and developed for the static regime, is related to the impossibility to locate the position of the crack and to predict the crack sizes. Moreover, the progressive degradation of stiffness material properties cannot be taken into account.

Plasticity approach can be appropriate for composites exhibiting ductile behavior (e.g. thermoplastic composites), in combination with the failure

criteria approach for damage prediction [14]. For such materials, a generalized anisotropic model in large strains, based on the classical isotropic plasticity theory, was presented by Car et al. [15].

The fracture mechanics approach [16] is based on the comparison of the strain energy at a crack front of known size with critical values of strain energy release rate. Zerbst et al. [17] applied this approach to predict residual compression strength and delamination growth in composites, showing appreciable results. The main disadvantage of fracture mechanics analysis is that it requires the definition of a pre-existing crack region in the numerical model.

The Continuum Damage Mechanics (CDM) approach, initially introduced by Kachanov [18] and Rabotnov [19], has grown considerably in the past twenty years. According to CDM, damage is considered as a deterioration process of the material, introduced as part of the material definition. Using CDM concept, Matzenmiller et al. [20] developed a mathematical model for damage of composite materials, connecting the damage level to the degraded elastic properties of the material, in turn depending on the particular damage mechanism (fibre breakage, fibre microbuckling, matrix cracking, etc.). This approach has been implemented in many research works [21-24], demonstrating promising results in predicting the impact response and damage extent.

SIGNIFICANCE AND SCOPES

Despite years of extensive research around the world, a complete and validated methodology for predicting the behavior of composite structures including the effects of damage has not yet been fully achieved. This is

largely due to the complexity of the physical phenomena involved, requiring an effective modelling of dynamic effects, material-projectile contact, failure modes development and interaction within the laminate, yet taking into account the influence of tup geometry, velocity, and mass, and target geometry, constraint conditions, and lay-up.

The scope of the present paper was to simulate the response of clamped circular GFRP plates of two different thicknesses, struck at low-velocity by a rigid hemispherical projectile. An FE model, based on the commercial tool LS-DYNA, was constructed and calibrated using the information gathered from a minimum of experimental data. The model was assessed by predicting the overall force-displacement (*F-d*) curve, the dissipated energy, and the shape and extent of delaminated area for unknown cases.

MATERIALS AND EXPERIMENTAL METHODS

The GFRP panels considered in this work were obtained from prepreg layers made of E-glass plain-weave fabric, 295 g/m^2 in areal weight, and Cycom 7701 epoxy resin. An overview of the mechanical properties of the ply material, drawn from the manufacturer's technical data sheet, is given in Tab. I (values in parentheses).

Two laminates, having stacking sequence $[(0,90)_n/(+45,-45)_n]_s$, with n=1,2 as depicted in Fig. 1, were obtained and press cured for 2 hours at 120°C temperature and 0.1 MPa pressure. The nominal thickness *t* was 0.96 mm and 1.92 mm for n=1 and n=2, respectively.

From the laminates, square specimens 70 mm in side were cut, and subjected to low-velocity impact tests using a Ceast MK4 instrumented testing machine, equipped with a DAS 4000 digital acquisition system. The

samples were clamped on a steel plate with a circular opening 50 mm in diameter, and struck at their centre using a hemispherical steel impactor, 16 mm in diameter and 3.6 kg in mass. Various energy levels *U*, in the range 0.4 to 20 J were adopted, appropriately setting the tup height. For each impact energy level, three experimental tests were performed.

Thanks to the translucent appearance of GFRP, the projected damage area A_p of selected impacted samples was highlighted by an intense light source located at their back side, photographed, and theA_p extent was measured through an image analyzer. Then, the specimens were immersed in a blue ink bath, until A_p was fully darkened; after that, they were carefully deplied with the help of moderate heating, and the extent of the delaminated areas found in correspondence of each interface was computed as the average measures of upper and lower delaminated areas of each ply, A_m; the total delaminated area, A_d, was computed as the sum of the delaminated surfaces in correspondence of each interface.

EXPERIMENTAL RESULTS AND DISCUSSION

Typical *F-d* curves recorded during the impacttests, obtained for the two panel thicknesses, are collected in Fig. 2.

At low displacement, the material behavior is substantially elastic, and disturbed by dynamic oscillations, more marked for the thicker panel. As discussed in previous works [25,26], the curvature affecting the thinner laminate during this step is due to membrane effects. Beyond a given load threshold, dependent on the target thickness, sudden load drops appear in the *F-d* curves, indicating damage beginning and propagation. Nevertheless, the general trend of the contact force increases further up to the maximum load,

where a dramatic load drop, suggesting major damage, is observed. After that, the *F-d* curves flatten out until the maximum displacement, corresponding to a zero velocity, is achieved. During rebound, the elastic portion of the energy stored into the material is transferred back to the impactor, whereas another portion (represented by the area enclosed in the *F-d* curve) is irreversibly absorbed through material damage, heat, and vibrations.

As previously specified, the different energy levels in the tests were obtained by suitably setting the drop height of the impactor, i.e. using different impact velocities. In Fig. 3, different *F-d* curves, deriving from impact tests performed at increasing energy levels, are superposed. Despite some obvious differences, attributable to the experimental scatter, the superposition is good. This indicates that, within the experimental conditions adopted in the present tests, the material response is not sensitive to velocity, so that energy is the true parameter affecting its response.

In Fig.4, the irreversibly absorbed energy U_d, measured as the area enclosed within the *F-d* curve, is plotted against *U* (full symbols). As also found by other researchers [26], the trend is sensibly linear, with a slightly higher rate characterizing the thinner laminate.

The visible delaminated area (Fig. 5) was diamond-shaped, with the principal axes coinciding with the warp-weft directions of the surface fabric layers (horizontal and vertical directions in the figure), along which fibre fracture was found.

Apparently, delamination extent of the impacted specimens was larger when observed by the back face of the panel. This feature was confirmed by the measurements carried out after deplying, which also revealed fibre fractures,

developing along the warp-weft directions, in the internal layers. However, for t=1.92 mm, delamination took place also between layers with the same orientation located at the mid-plane of the laminate, as shown by the black symbols in Fig. 6, where the extent of ply-by-ply delaminated area A_m is diagrammed for U=20.0 J.In particular, the average measured delaminated area was 251.53 mm^2 and 482.80 $mm^2$for the interface between layers (0;90)/(-45;+45) and (-45;+45)/(0;90) respectively, with the latter ≈ 92% larger than the former. Thisdamage was expected since the interfaces between layers having different orientations are more prone to delamination, with the largest delaminated area located near the back face of the panelas often found in several impact studies [3,8,35]. Nevertheless, should be remarked that the amount of damage occurred at the mid-plane of the laminate, i.e. between layers with the same orientation (-45;+45)/(-45;+45),although smaller than the others (105.83 mm^2),is of the same order of magnitude compared with the other delaminatedinterfaces.

Of course, damage extent increased monotonically with increasing impact energy. This is shown in Figs. 7and 8(full symbols), where the mean value d of the axes indicated by d_1, d_2 in Fig. 5, and the extent of projected delaminated area, A_p, are plotted, respectively, against U.

NUMERICAL ANALYSIS

Model features

The impact tests were simulated using the commercial finite element code LS-DYNA Version 971, and were run in double precision mode. Since one of the scopes of the analysis was the prediction of damage development, a 3D model of the ply was selected, to obtain a more accurate description of

the stress distribution along the ply thickness. Each ply was modelled through a single layer of three-dimensional eight nodes finite elements, whereas the bond between adjacent plies was simulated through distributed spring connections. The whole laminate model consists of 4 (for t=0.96mm laminate) and 8 (t=1.92mm) discrete circular plates 50mm in diameter, representing each single fabric ply arranged according to the fixed lay-up sequence.

The elements had an edge length along the thickness corresponding to the thickness of a single ply, i.e. 0.24 mm. A parametric study was carried out, investigating the influence of the plane element lengths showing a mesh dependency. Specifically, the composite material failure behaviour is influenced by the element size affecting the absorbed energy which varies with the element length and converges for small elements dimensions. Moreover, since the impact of the rigid hemisphere is very localized, a very fine mesh is required in order to achieve an accurate mechanical behaviour and a correct working of the contact algorithm.The selected in-plane element edge lengths were approximately 0.657 mm and the 90% of elements had an aspect ratio of 3:1 or less.

Among the lamina constitutive models available in LS-DYNA, the Mat Composite Failure Option Model (Mat 059, Option = Solid) [27], able to model the progressive damage of the material on the basis of a three-dimensional stress-based failure criterion, was chosen in this work. Although the selection of MAT59 in shell formulation has been discussed in several applications available in literature[28], works or detailed descriptions investigating its behavior in 3D formulations are scarce and only few information can be found from informal documentation available

from Livermore Software Technology Corp. (LSTC); nevertheless authors verified the behavior of the constitutive model through single element analysis.In particular, the composite failure model MAT059 simulates the 3-dimensional behavior of an orthotropic composite material and its progressive failure due to any of several failure criteria. The 3-D constitutive model is based on orthotropic elasticity up to failure, according to the following equation:

$$[C]\{\sigma\} = \{\varepsilon\} \quad (1)$$

being:

$$[C] = \begin{bmatrix} \frac{1}{E_{11}} & -\frac{\nu_{12}}{E_{22}} & -\frac{\nu_{13}}{E_{33}} & 0 & 0 & 0 \\ -\frac{\nu_{21}}{E_{11}} & \frac{1}{E_{22}} & -\frac{\nu_{23}}{E_{33}} & 0 & 0 & 0 \\ -\frac{\nu_{31}}{E_{11}} & -\frac{\nu_{32}}{E_{22}} & \frac{1}{E_{33}} & 0 & 0 & 0 \\ 0 & 0 & 0 & \frac{1}{G_{23}} & 0 & 0 \\ 0 & 0 & 0 & 0 & \frac{1}{G_{31}} & 0 \\ 0 & 0 & 0 & 0 & 0 & \frac{1}{G_{12}} \end{bmatrix}$$

the compliance matrix, where 1 and 2 are the in plane directions, and

$$\{\sigma\} = \begin{Bmatrix} \sigma_{11} \\ \sigma_{22} \\ \sigma_{33} \\ \sigma_{23} \\ \sigma_{31} \\ \sigma_{12} \end{Bmatrix}, \quad \{\varepsilon\} = \begin{Bmatrix} \varepsilon_{11} \\ \varepsilon_{22} \\ \varepsilon_{33} \\ \gamma_{23} \\ \gamma_{31} \\ \gamma_{12} \end{Bmatrix}$$

the six stress and strain components respectively.

The presented material model implements a stress based failure criterion for solid elements derived by the Tsai-Wu theory [29], able to predict the onset of the major failure modes, including:

- longitudinal and transverse tensile failure,
- longitudinal and transverse compressive failure,
- through the thickness compressive failure, and

- through the thickness shear failure.

In example, the longitudinal tensile failure is reached when the following relationship is fulfilled:

$$\left(\frac{\sigma_{11}}{X_t}\right)^2 + \left(\frac{\sigma_{12}}{S_{12}}\right)^2 + \left(\frac{\sigma_{13}}{S_{13}}\right)^2 \geq 1 \quad (2)$$

being σ_{11}, σ_{12} and σ_{13} the longitudinal, in plane shear and out of plane shear stress components and X_t, S_{12} and S_{13} the corresponding strength values. When the criterion is satisfied, the corresponding stiffness (and consequently the load carrying capability of the material in that direction) is degraded to zero over a small computational time, corresponding to a rapid decay of the stress-strain relationship; hence, the compliance matrix progressively reduces to:

$$[C] = \begin{bmatrix} 0 & 0 & 0 & 0 & 0 & 0 \\ 0 & \frac{1}{E_{22}} & 0 & 0 & 0 & 0 \\ 0 & 0 & \frac{1}{E_{33}} & 0 & 0 & 0 \\ 0 & 0 & 0 & 0 & 0 & 0 \\ 0 & 0 & 0 & 0 & 0 & 0 \\ 0 & 0 & 0 & 0 & 0 & 0 \end{bmatrix}$$

The other failure modes act similarly according to threshold stress criteria, as that introduced in equation (2). Failure criteria act independently contributing to an ultimate failure of the composite system, that is, once a failure criterion is attained, degradation occurs only in the corresponding direction without affecting the other stress criteria computation. Element is removed from the calculation when the failure is attained in all the directions and can no longer carry any load.The input parameters needed for

this material formulation are the orthotropic elastic parameters and the threshold values of the critical stresses for failure criteria.

Delamination modelling

Delamination damage was implemented in the simulation model through the use of a surface-to-surface tiebreak contact algorithm based on the knowledge of the interlaminar properties of the material in terms of normal and shear strengths. Among the different formulations available in LS-DYNA, the penalty contact formulation contact-automatic-one-way-surface-to-surface-tiebreak with failure law option 6 [27] was adopted between separate solid elements modelling solid plies. Using this approach, each ply is modelled as a solid layer of elements, but the nodes between plies initially in contact are tied together, inhibiting sliding motions, until a failure criterion is reached, corresponding to delamination onset. In particular, the nodal stress is monitored throughout the analysis and implemented in the interface strength-based failure criterion:

$$\left(\frac{|\sigma_n|}{NFLS}\right)^2 + \left(\frac{|\sigma_s|}{SFLS}\right)^2 \geq 1 \qquad (3)$$

where σ_n and σ_s are the current normal and shear stresses, respectively, and NFLS, SFLS the normal and shear interlaminar strengths to be set in the contact definition.

When Eq. (3) is fulfilled, contact stress is linearly reduced to zero as a function of the distance between two points initially in contact. As soon as a defined critical crack opening (CCRIT) is reached, the tie contact definition for those nodes is released. Once the tie component of the contact definition is deleted, the contact for those nodes converts into a standard surface-to-surface definition preventing interpenetration.

The impactor was modelled as a hemispherical rigid body with rigid LS-DYNA material model (MAT-RIGID). Its initial velocity and mass were set depending on the energy level considered. Contact between the impactor and the whole laminate was simulated using the AUTOMATIC-SURFACE-TO-SURFACE penalty based contact algorithm.

Ply element deleting criterion was added by using ADD-EROSION card, which allows elements to be deleted from the calculation if a certain condition based on values of stress, strain, pressure, etc. are met; in particular, a strain condition was set as a deleting criterion on the basis of reasonable maximum principal strain and shear strain values occurring at fibre and matrix failure, in order to avoid excessive distortion of failed elements and consequent instabilities of the finite elements. A stiffness-based hourglass control was employed to improve the deformation behavior of the elements. The outer boundaries of the plates were considered to be clamped. Geometric and material symmetry allowed the analysis of one-quarter of the impactor and of the plate, as depicted in Fig. 9.

ASSESSMENT OF THE MODEL

The mechanical properties needed for MAT059 concern elastic moduli along the three principal directions, in-plane tensile, compressive and shear strength values, and interlaminar failure stresses (NFLS, SFLS). Only some of the input parameters requested for the numerical analysis were available from the manufacturer's data sheet (values in parentheses in Table I), so that a calibration procedure was followed to assign the unknown properties. In this section, first, some details on the calibration stage are given; then, the

main topics of the work, i.e. predicting the *F-d* curve, and calculating the shape and extent of delaminated zone, are addressed separately.

Calibration Analysis

A sensitivity analysis showed that, within a quite large range of values, the influence of the Poisson's ratios on the elastic response of the panels is negligible. Typical values, deriving from those adopted in [30,31], where then employed in the calculations. The structural response was more sensitive to the through-the-thickness Young's modulus, E_3, as well as to the shear moduli. To find reasonable values for these parameters, the *F-d* curve recorded for U=0.41 J, t=0.96 mm (Fig. 10a), developing in the elastic range, was considered, and the constants E_3, G_{12}, $G_{13}=G_{23}$ were calibrated requiring a satisfactory superposition of the predicted to the experimental curve.

The sensitivity analysis also revealed that the compression strengths $X_C=Y_C$ do not sensibly affect the trend of the *F-d* curve. On the contrary, the first failure point (signaled by an evident load drop in the *F-d* curve) is critically dependent on $X_T=Y_T$, S_{12}, and *NFLS*. Assuming a value similar to the one adopted in [30] for S_{12}, X_T and *NFLS* were determined from the *F-d* curves concerning U=1.55 J, t=0.96 mm (Fig. 10b), imposing that: a) the experimental displacement in correspondence of which first failure was found would be coincident with the numerical one; b) after load drop at first failure, the trend of the calculated and actual curve would overlap.

The calibrated values used in the numerical model are reported in Tab. I. Comparing them with the properties drawn from the producer's data sheet (in parentheses in the table), $X_T=Y_T$ is more than doubled. This is somehow

anticipated, since the strength of GFRP is particularly sensitive to loading rate. Caprino et al. [32], conducting low-velocity impact tests on glass-polyester plates, noted a 70% increase in the maximum contact force with respect to static loading. Sims [33] reported an increase in flexural strength for glass mat/polyester laminates in the speed range 10^{-6} to 10^{-1} ms^{-1}, while Asprone et al. [34] recorded an improvement in tensile mechanical properties in pultruded glass-polyester composites at strain rates ranging from 1 s^{-1} to 700 s^{-1}.

F-d curves

In Figs. 10and 11, the experimental *F-d* curves(continuous lines) recorded at different impact energy levels are compared with those obtained by numerical analysis (dashed lines) for t=0.96 mm and t=1.92 mm, respectively.

The agreement between experiments and FE in Figs 10a, b in the loading phase is obvious, since some information gathered from these curves was used to calibrate the numerical model. However, the general trend of all other (completely unknown) curves is reasonably well captured by FE, not only in the loading, but also in the unloading stage of contact history. In particular, the elastic response of the thicker laminate (Fig. 11a) is predicted with excellent accuracy.

Indeed, two major phenomena, evident when the thicker laminate is considered (Fig. 11), distinguishing the numerical solutions from the actual cases: the oscillations pertaining to the elastic phase are not accurately described, and the predicted sudden load drops deriving from failures are much larger than observed. The first event is anticipated: since the *F-d* curve

was verified to be substantially insensitive to velocity (Fig. 3), the initial impact velocity V was held constant in the FE model (V=50 mm/s),and energy was set by suitably selecting the impactor mass. Consequently, the main features correlated with impact dynamics were lost.

The entity of sudden load drops in the numerical *F-d* curve, determined by damage propagation, is critically dependent on the ability to effectively model the progressive damage within the ply, as well as the laminate response after Eq. (3) has been fulfilled. Probably, a more sophisticated law describing the behaviour of tiebreak elements would be required to better reproduce the actual material behaviour.

The open symbols in Fig. 4represent the absorbed energy provided by FE analysis. The numerical values match satisfactorily the experimental data (full symbols), especially for small energy values. In particular, the FE simulations reproduce well both the linear dependence of U_d on impact energy and the effect of the thickness on the slope of the straight line. With increasing U, the FE predictions tend to underestimate U_d. Of course, this reflects the approximations implicit in the modelling of material behaviour during progressive damage.

Damage assessment

As previously specified, the simulation results indicate where interlaminar failures occur in terms of nodal restraint failures. In particular, once the failure criterion is reached, the force in contact restraint is linearly scaled down to zero. Then, nodal connection fails completely and nodal restraint is removed. Through the identification of the released node restraints, the

delamination mapping can be defined for each laminate interface, in order to quantify interlaminar damage.

The open symbols in Fig. 7represent the characteristic length *d* of the delaminated area provided by FE. Indeed, the numerical values are very close to the experimental ones (full symbols), confirming the reliability of FE model. Similar conclusions can be drawn from Fig. 8, where the comparison between FE and measured values is carried out referring to the projected delaminated area, A_p.

Further support to the numerical results is given in Fig. 12, where a view of the bottom face of a damaged plate is illustrated (Fig. 12a). In Fig. 12b, the FE mesh of the portion enclosed within the dashed line in Fig. 12a is shown; the bright area represents delamination, as predicted by the FE model. Clearly, not only the dimensions, but also the overall shape of delaminated area are well predicted by FE.

In order to more deeply evaluate the capability of the model to estimate delamination, a comparison between the extent of experimentally determined and predicted ply-by-ply delaminated areas was carried out. An example of the results obtained is shown in Fig. 6, where the open symbols refer to FE.

The general trend of delamination development within the laminate is well reproduced by the numerical analysis. In particular, as often found in impact studies [3,8,35], the interfaces between layers having different orientations are recognized to be more prone to delamination, with the largest delaminated area located near the back face of the panel. Further, in agreement with the experimental observations, FE indicates that the critical conditions for delamination are also reached at interfaces between laminae

with the same orientation. Among the latter, the mid-plane is correctly predicted to suffer the most extensive propagation.

It is interesting to note that, when interlaminar surfaces between layers having the same orientation are concerned, the delamination extent calculated by FE is larger than its actual counterpart (Fig. 6). A possible explanation is in the fact that, in the numerical analysis, the same interlaminar strength was assigned to all the interlayers. Probably, better agreement between experiments and calculated values could be achieved by assuming the normal and shear failure stresses at the interfaces as dependent on the relative orientations of the adjacent laminae.

CONCLUSIONS

Low-velocity impact tests were carried out on glass fabric/epoxy laminates, adopting two panel thicknesses and different impact energies. The experimental tests were modelled through the explicit FE software LS-DYNA.

From the results obtained, FE estimated with sufficient accuracy the overall force-displacement curve during the loading and rebound phases, as well as the irreversibly absorbed energy. Satisfactory agreement between numerical predictions and experiments was also verified with reference to the extent and shape of projected and ply-by-ply delaminated areas. In particular, as confirmed by the “post-mortem” analysis of the impacted panels, FE calculated considerable delamination at the interface located at the mid-plane of the specimens, characterized by two layers having same orientation. In general, the predicted delamination extent between laminae of identical orientation was larger than the actual one. Probably, this depends on the

interlaminar strengths assigned in the calculations, which were assumed independent of the relative orientations of adjacent plies.

REFERENCES

[1] Abrate S, Impact on composite structures, Cambridge University Press, 1998.

[2] Sjoblom PO, Hartness JT, Cordell TM, "On low-velocity impact testing of composite materials", *J Compos Mater*, 22, 1988, 30-52.

[3] Richardson MO W, Wisheart MJ, "Review of low-velocity impact properties of composite materials", *Composites Part A*, 27A, 1996, 1123-1131.

[4] Shim VPW, Yang LM, "Characterization of the residual mechanical properties of woven fabric reinforced composites after low-velocity impact", *Int J MechSci*, 47, 2005, 647-665.

[5] Chen JK, Sun CT, "Dynamic large deflection response of composite laminates subjected to impact", *Compos Struct*, 4, 1985, 59-73.

[6] Caprino G, Langella A., Lopresto V, "Elastic behaviour of circular composite plates transversely loaded at the centre", *Composites Part A*, 33, 2002, 1191-1197.

[7] Olsson R, "Analytical prediction of large mass impact damage in composite laminates", *Composites Part A*, 32, 2001, 1207-1215.

[8] Naik NK, Chandra Y, "Damage in woven-fabric composites subjected to low-velocity impact", *Compos SciTechnol*, 60, 2000, 731-744.

[9] Sutherland LS, GuedesSoares C, "Effect of laminate thickness and of matrix resin on the impact of low fibre-volume, woven roving E-glass composites", *Compos SciTechnol*, 64, 2004, 1691-1700.

[10] Zhou G, "The use of experimentally-determined impact force as a damage measure in impact damage resistance and tolerance of composite structures", *Compos Struct*, 42, 1998, 375-382.

[11] Abrate S, "Modeling of impacts on composite structures", *Compos Struct*, 51, 2001, 129-138.

[12] Olsson R, Donadon MV, Falzon BG, "Delamination threshold load for dynamic impact on plates", *Int J Solids Struct*, 43, 2006, 3124-3141.

[13] Jones RM, Mechanics of composite materials, 2nd ed, Taylor and Francis, 1999.

[14] Olsson MD, Varizi R, Anderson DL, "Damage in composites: a plasticity approach", *J Compos Mater*, 44, 1992, 103-116.

[15] Car E, Oller S, Onate E, "A large strain plasticity model for anisotropic materials – composite material application", *Int J Plasticity*, 17, 2001, 1437-1463.

[16] Garg AC, "Delamination - a damage mode in composite structures", EngngFractMech, 29, 1988, 557-584.

[17] Zerbst U, Heinimann M, Dalle Donne C, Steglich D, "Fracture and damage mechanics modeling of thin-walled structures – An overview", *EngngFractMech*, 76, 2009, 5-43.

[18] Kachanov LM, "Time of rupture process under creep conditions", *IzyAkadNank SSR Otd Tech Nauk*, 1958, 8, 26-31.

[19] Rabotnov YN, Creep Problems in Structural Members, North-Holland, Amsterdam, 1969.

[20] Matzenmiller A, Lubliner J, Taylor RL, "A constitutive model for anisotropic damage in fibre-composites", *Mech Mater*, 20, 1995, 125-152.

[21] Williams VK, Varizi R, Poursartip A, "A physically based continuum damage mechanics model for thin laminated composite structures", *Int J Solids Struct*, 40, 2003, 2267-2300.

[22] Iannucci L, "Progressive failure modeling of woven carbon composite under impact", *Int J Impact Engng*, 32, 2006, 1013-1043.

[23] Donadon MV, Iannucci L, Falzon BG, Hodgkinson JM, Almeida SFM, "A progressive failure model for composite laminates subjected to low velocity impact damage", *ComputStruct*, 86, 2008, 1232-1252.

[24] Lopes CS, Camanho PP, Gürdal Z, Maimí P, González EV, "Low-velocity impact damage on dispersed stacking sequence laminates. Part II: Numerical simulations", *Compos SciTechnol*, 69, 2009, 937-947.

[25] Shivakumar KN, Elber W, Illg W, "Prediction of impact force and duration due to low-velocity impact on circular composite laminates", *J ApplMech*, 52, 1985, 674-80.

[26] Sutherland LS, GuedesSoares C, "Impact of low fibre-volume, glass/polyester rectangular plates", *Compos Struct*, 68, 2005, 13-22.

[27] LS-DYNA Keyword User's Manual, Livermore Software Technology Corporation, Version 971, May 2007.

[28] Schweizerhof K, "Crashworthiness analysis with enhanced composite material models in LS-DYNA – merits and limits", LS-DYNA World Conference,1998, Detroit, Michigan, USA.

[29]Tsai SW and Wu EM, "A general theory of strength for anisotropic materials," J. Comp. Mater. 5, 1971, 58-80

[30] Gama BA, Bogetti TA, Gillespie JW Jr., " Progressive Damage Modeling of Plain-Weave Composites using LS-Dyna Composite Damage Model MAT162", 7th Europ. LS-DYNA Conf.,D-III-04.

[31] Sevkat E, Liaw B, Delale F, Raju BB, "Drop-weight impact of plain-woven hybrid glass–graphite/toughened epoxy composites", *Composites Part A*, 40, 2009, 1090-1110.

[32] Caprino G, Crivelli Visconti I, Di Ilio A, "Composite materialresponse under low-velocity impact", *ComposStruct*, 2, 1984, 261-271.

[33] Sims, GD, "Understanding Charpy impact testing of composite laminates", Proc. 6th Int. Conf. on Composite Materials and 2nd European Conf. on Composite Materials', Imperial College, London, 1988, 3494-3507.

[34] Asprone D, Cadoni E, Prota A, Manfredi G, "Strain-rate sensitiveness of a pultruded e-glass/polyester composite", *J Compos Construct*, 13, 2009, 558-564.

[35]Wu HYT, Springer GS,"Measurements of matrix crackingand delamination caused by impact on composite plates",*J Compos Mater*,22, 1988, 518-532.

FIGURES CAPTIONS

Fig. 1 – Schematic representation of the stacking sequence.

Fig. 2– Effect of the laminate thickness, *t*, on the *F-d* curves.

Fig. 3– Effect of the energy level, *U*, on the *F-d* curves. Laminate thickness t=0.96mm.

Fig. 4- Absorbed energy, U_d, vs impact energy, *U*.

Fig. 5– Visible damage area of an impacted panel.

Fig. 6- Extent of ply-by-ply delaminated area, A_m. Panel thickness *t*=1.92mm; impact energy *U*=20.0 J.

Fig. 7– Characteristic dimension of projected delaminated area, *d*, vs impact energy, *U*.

Fig. 8- Projected delaminated area, A_p, vs impact energy, *U*.

Fig. 9- FE model set up adopted in the numerical analysis.

Fig.10 - Comparison of experimental and numerical *F-d* curves for the 0.96 mm thick laminate; a) *U*=0.4J; b) *U*=1.5J; c) *U*=3.3J; d) *U*=4.0J; e) *U*=6.0J.

Fig. 11 - Comparison of experimental and numerical *F-d* curves for the 1.92 mm thick laminate; a) *U*=0.8J; b) *U*=8.3J; c) *U*=12.4J; d) *U*=15.5J.

Fig. 12 - Comparison of: a) experimental, and, b) calculated delaminated area. Laminate thickness *t*=0.96 mm; impact energy *U*=6.0 J.

Table 1– Mechanical properties of the calibrated model

Elastic Moduli	(GPa)	Shear Moduli	(GPa)	Poisson ratios	(-)
E_1	26 (26)	G_{12}	3.8	v_{12}	0.1
E_2	26 (26)	G_{23}	2.8	v_{13}	0.25
E_3	8	G_{13}	2.8	v_{23}	0.25
Tensile strengths	(MPa)	*Compressive strengths*	(MPa)	*Shear strengths*	(MPa)
X_T	850 (414)	X_C	720 (458)	S_{12}	105
Y_T	850 (414)	Y_C	720 (458)	S_{13}	65 (65)
Z_T	120	Z_C	500	S_{23}	65 (65)

Interlaminar Normal Failure Stress	(MPa)	Interlaminar Shear Failure Stress	(MPa)
NFLS	35	*SFLS*	65 (65)

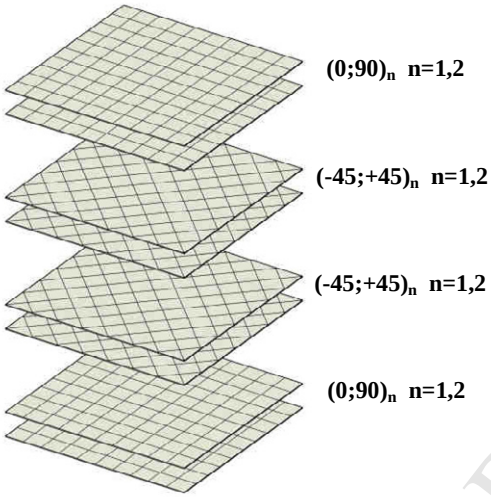

Fig. 1 – Schematic representation of the stacking sequence.

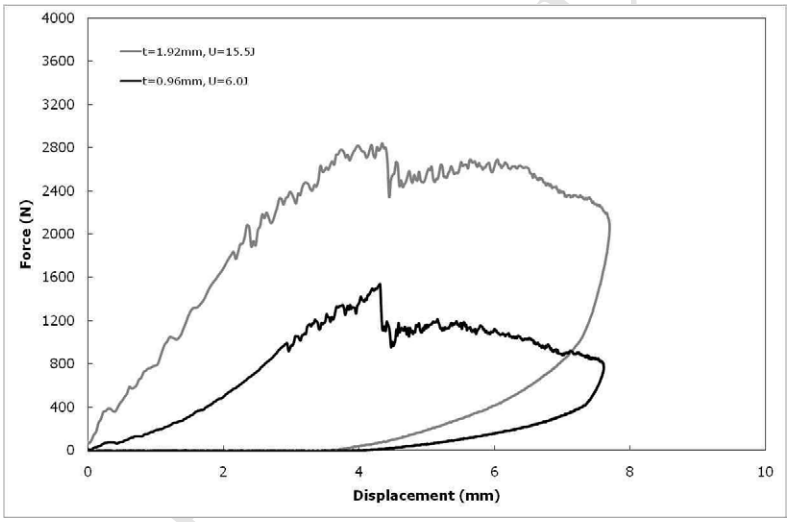

Fig. 2– Effect of the laminate thickness, *t*, on the *F-d* curves.

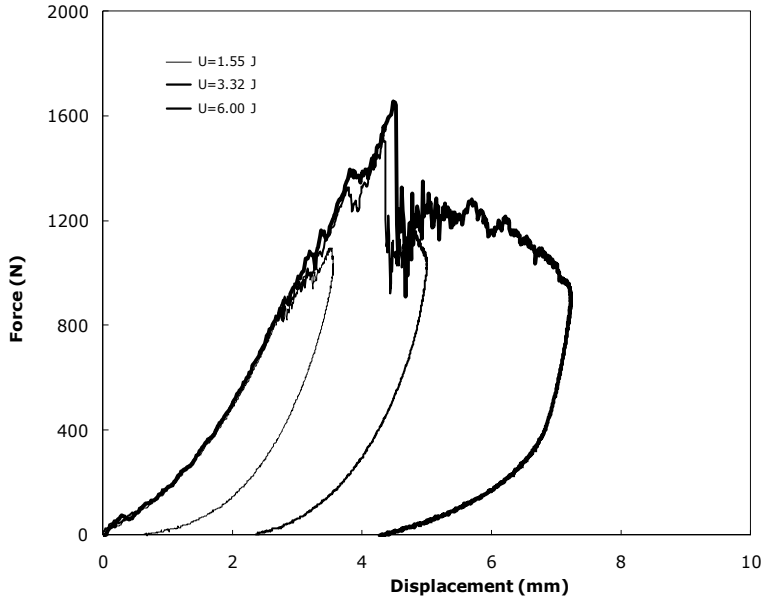

Fig. 3– Effect of the energy level, *U*, on the *F-d* curves. Laminate thickness *t*=0.96mm.

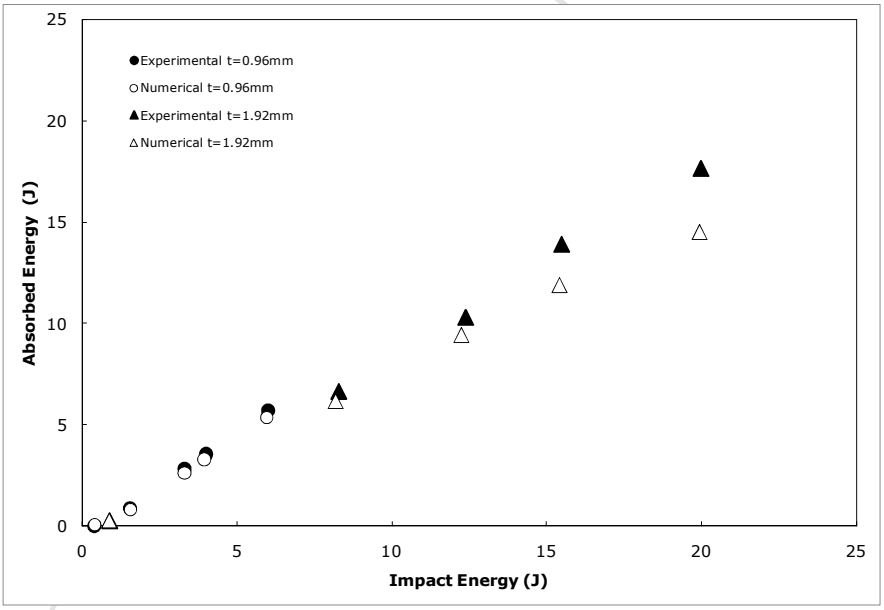

Fig. 4- Absorbed energy, U_d, vs impact energy, *U*.

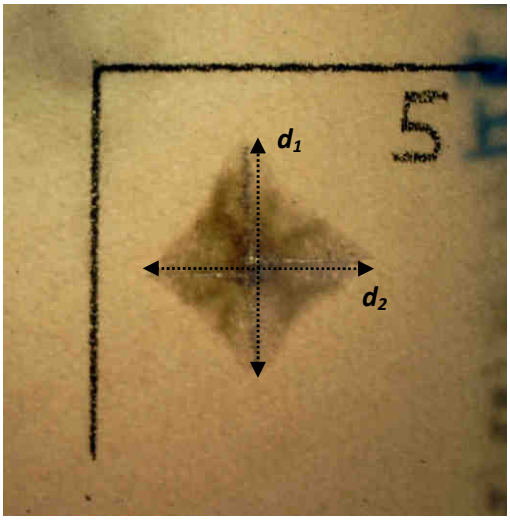

Fig. 5– Visible damage area of an impacted panel.

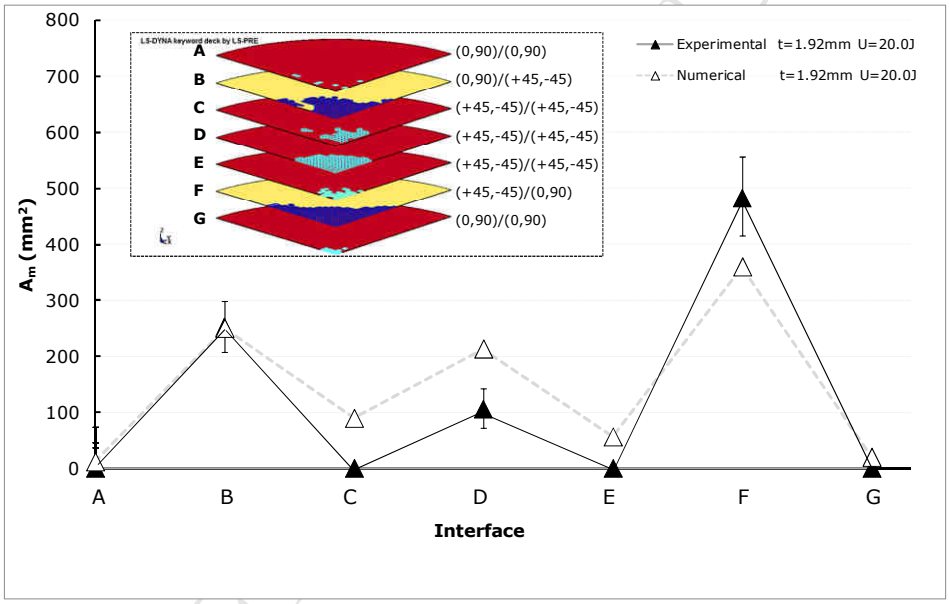

Fig. 6- Extent of ply-by-ply delaminated area, A_m. Panel thickness t=1.92mm; impact energy U=20.0 J.

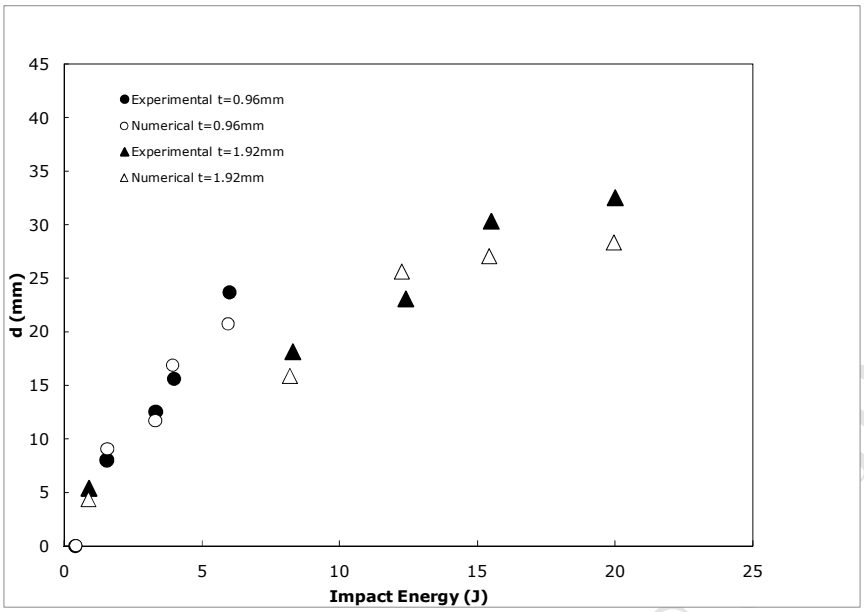

Fig. 7– Characteristic dimension of projected delaminated area, *d*, vs impact energy, *U*.

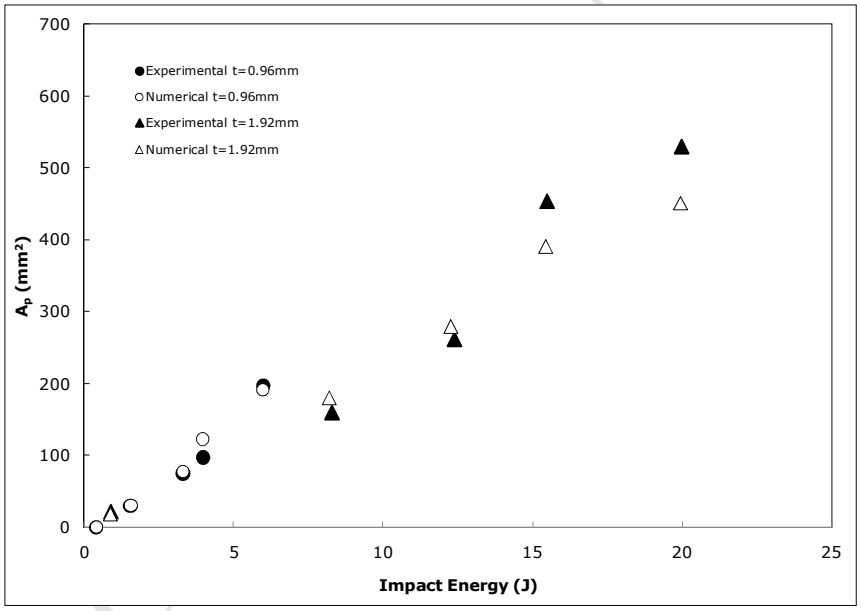

Fig. 8- Projected delaminated area, A_p, vs impact energy, *U*.

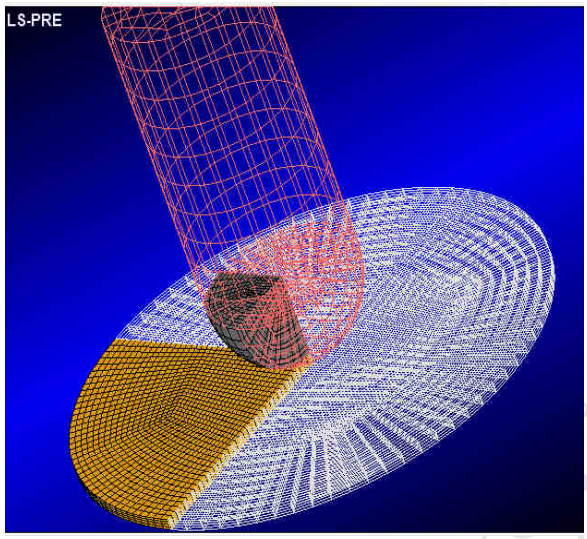

Fig. 9- FE model set up adopted in the numerical analysis.

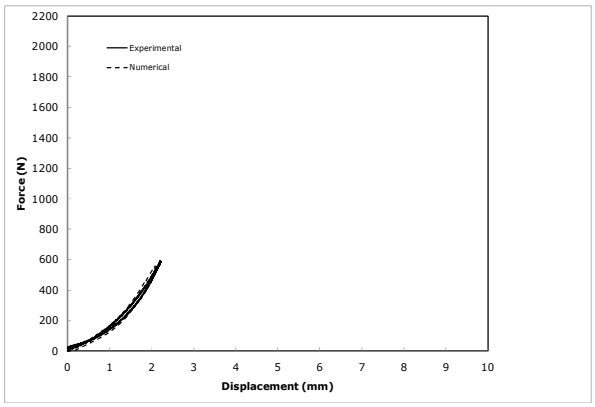

a)

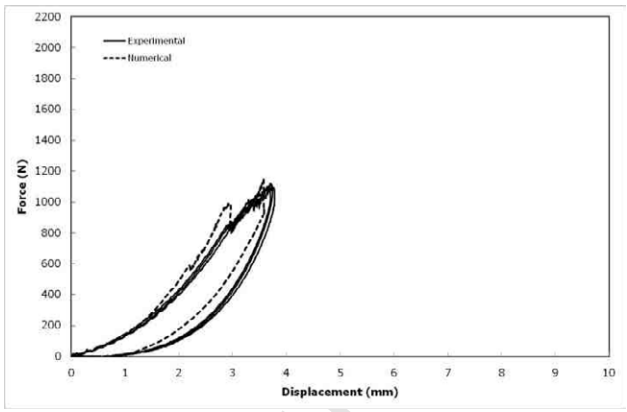

b)

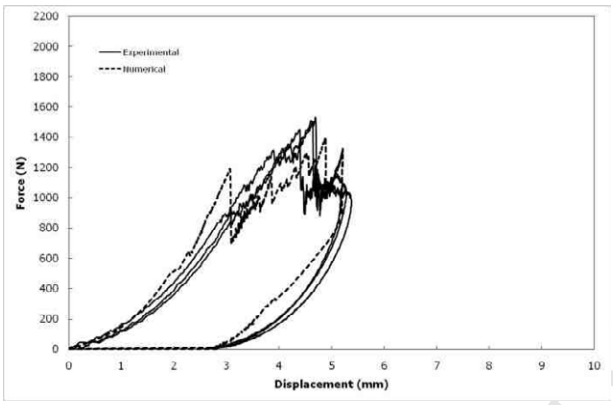

c)

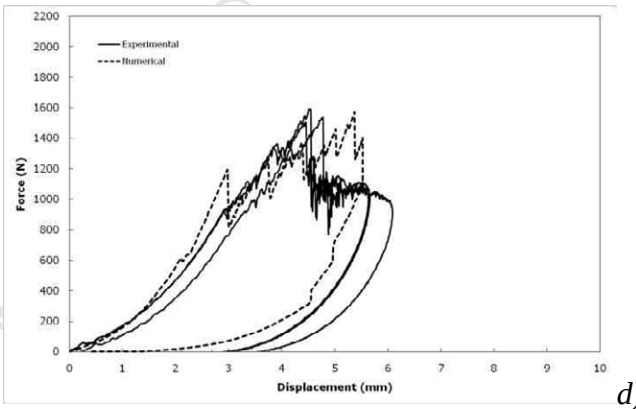

d)

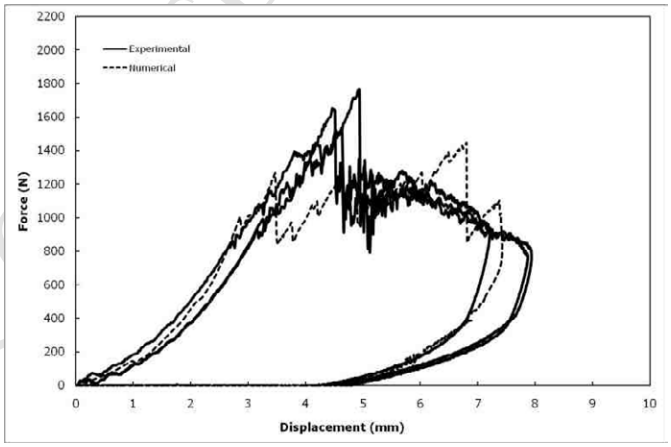

e)

Figure 10- Comparison of experimental and numerical *F-d* curves for the 0.96 mm thick laminate; a) *U*=0.4J; b *U*=1.5J; c) *U*=3.3J; d) *U*=4.0J; e) *U*=6.0J.

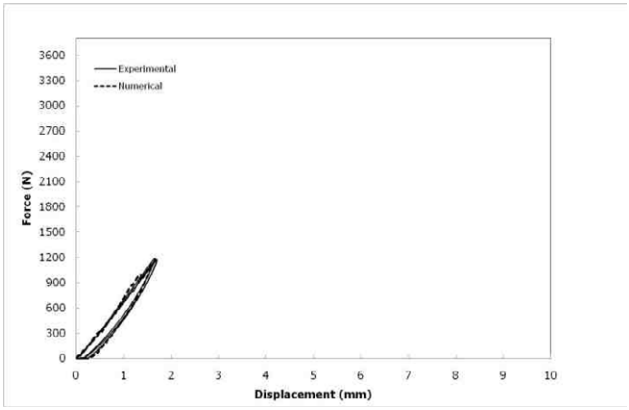

a)

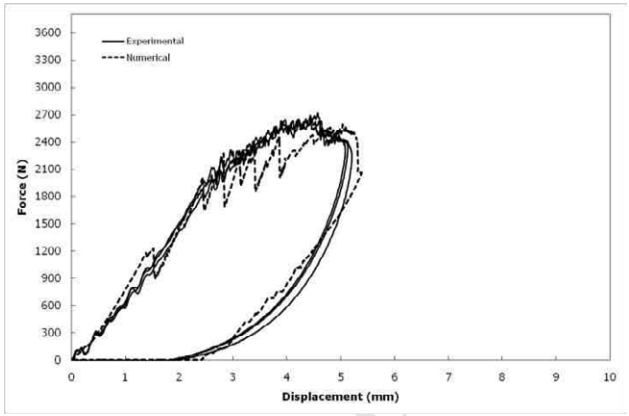

b)

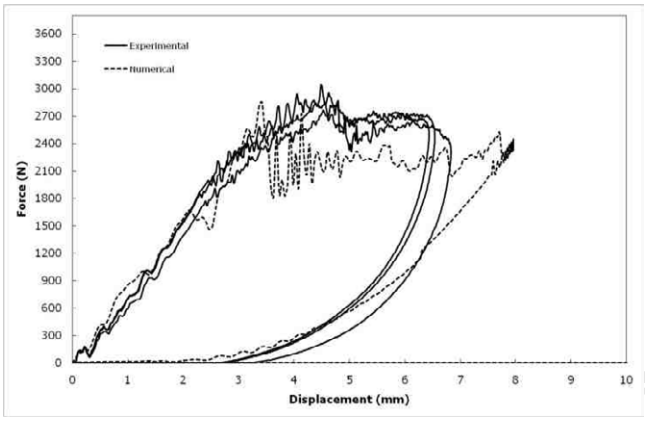

c)

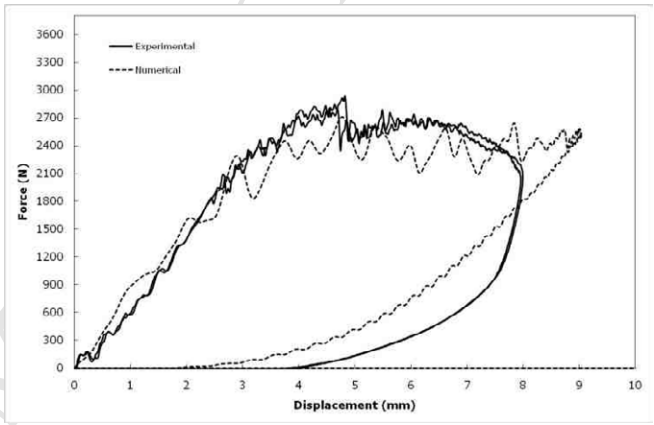

d)

Figure 11- Comparison of experimental and numerical *F-d* curves for the 1.92 mm thick laminate; a) *U*=0.8J; b) *U*=8.3J; c) *U*=12.4J; d) *U*=15.5J.

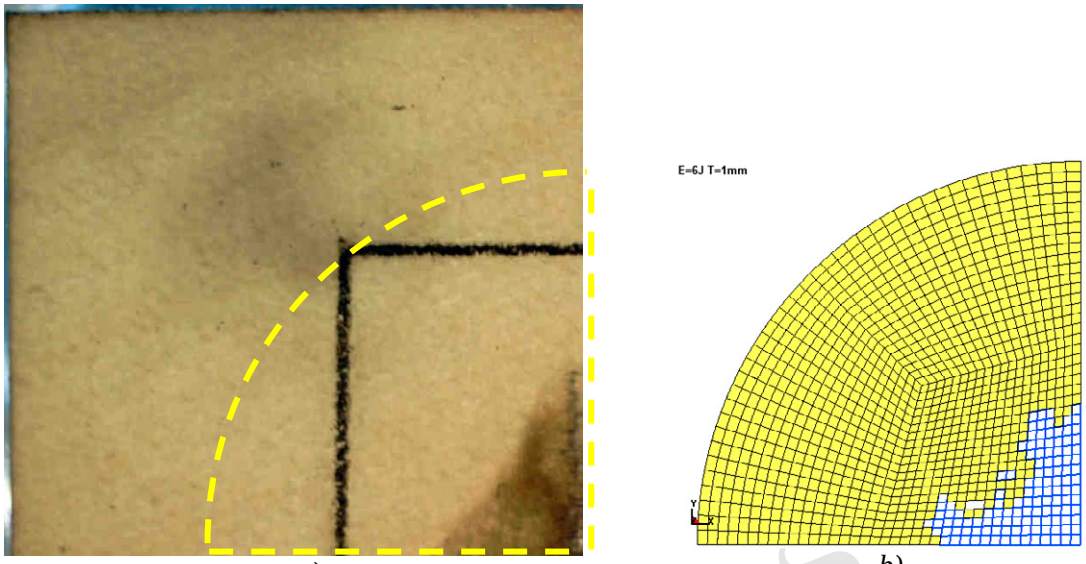

Fig. 12- Comparison of: a) experimental, and, b) calculated delaminated area. Laminate thickness t=0.96 mm; impact energy U=6.0 J.